NOTE

Image resampling effects

Image resampling effects in mammographic image simulation

M Yip[1], A Mackenzie[2], E Lewis[1], D R Dance[2,3], K C Young[2,3], W. Christmas[1] and K Wells[1,4]

[1] Centre for Vision, Speech and Signal Processing, Faculty of Engineering and Physical Sciences, University of Surrey, Guildford, Surrey, GU2 7XH, UK.
[2] National Coordinating Centre for the Physics of Mammography, Royal Surrey County Hospital, Guildford, Surrey, GU2 7XX, UK
[3] Department of Physics, Faculty of Engineering and Physical Sciences, University of Surrey, Guildford, Surrey, GU2 7XH, UK
[4] King Saud University, Riyadh, Saudi Arabia

E-mail: mary.yip@surrey.ac.uk

Abstract. This work describes the theory of resampling effects within the context of image simulation for mammographic images. The process of digitization associated with using digital imaging technology needs to be correctly addressed in any image simulation process. Failure to do so can lead to overblurring in the final synthetic image.

A method for weighted neighbourhood averaging is described for non-integer scaling factors in resampling images. The use of the method is demonstrated by comparing simulated and real images of an edge test object acquired on two clinical mammography systems. Images were simulated using two setups: from idealised images and from images obtained with clinical systems. A Gaussian interpolation method is proposed as a single step solution to modelling blurring filters for the simulation process.

PACS numbers: 87.57.C, 87.57.cf, 87.57.cp

Submitted to: *Phys. Med. Biol.*

1. Introduction

Simulation of mammographic (and other radiographic) images is of growing interest to the biomedical imaging community (Saunders & Samei 2003, Workman 2005, Båth et al. 2005, Grosjean & Muller 2006, Gong et al. 2006, Zhou et al. 2007). In addition to the well known Monte Carlo physics simulation methods, there are two principal approaches that may be employed for image simulation: (a) synthesising artificial images from a (virtual) idealised noiseless template/test object to which noise is then added (Saunders & Samei 2003, Yip et al. 2008); (b) synthesising derived images of one particular imaging system using one or more images produced from another system(Workman 2005, Carton et al. 2005, Zanca et al. 2008, Mackenzie et al. 2011). Such image simulation methods can be used as an effective method of assessing and optimising image acquisition settings (Workman 2005, Båth et al. 2005, Grosjean & Muller 2006, Gong et al. 2006, Samei et al. 2007, Ruschin et al. 2007), or as a powerful tool where there is difficulty obtaining statistically significant image numbers for clinical observer trials (Samei et al. 2007, Ruschin et al. 2007, Zanca et al. 2008). In such studies, one needs to be confident that any modification to the original image data does not introduce new image artefacts.

The scope of this note is confined to the theoretical influence of the intrinsic blurring of the point spread function as represented by the modulation transfer function (MTF) and the subsequent effects of the discretization function or pixel sampling upon image simulation. To our knowledge, the effects of these two components have not been considered in detail before in the context of image simulation. Previous work, for example, assumed that blurring effects due to resampling are either negligible or encompassed in the resampling process(Carton et al. 2005, Zanca et al. 2008). Here we offer a formalism for resolution modification, taking account of both of these factors: namely, changes in detector blur (MTF) and pixel size, which is then studied using simulated and experimental data.

2. Method

2.1. Description of the physical imaging process

In an analogue linear system, the idealised input image, $f(x, y)$, is related to the output image, $g(x, y)$, through the following relationship(Gonzalez & Woods 2008).

$$g(x, y) = h(x, y) \star f(x, y) + \eta(x, y) \tag{1}$$

where $h(x, y)$ is the spatial representation of some image degradation function which is convolved ($\star$) with the idealised input image and stochastically degraded by a noise component, $\eta(x, y)$‡, to give the output image, $g(x, y)$. Within the context of the image space (x, y), $h(x, y)$ can be considered as the point spread function (PSF) of the

‡ $\eta(x, y)$, may be correlated with $h(x, y)$ depending on the imaging system

detector. Assuming shift invariance, then convolution in the spatial domain is equivalent to multiplication in the frequency domain, Equation 1 can be rewritten as:

$$G(u,v) \simeq H(u,v).F(u,v), \tag{2}$$

where $F(u,v)$ represents the Fourier Transform of the '*idealised image*', i.e. $f(x,y)$, and $H(u,v)$ can be considered to be the MTF of the detection system. As this note is concerned only with signal, the effects of additive noise are approximated as shown in Equation 2.

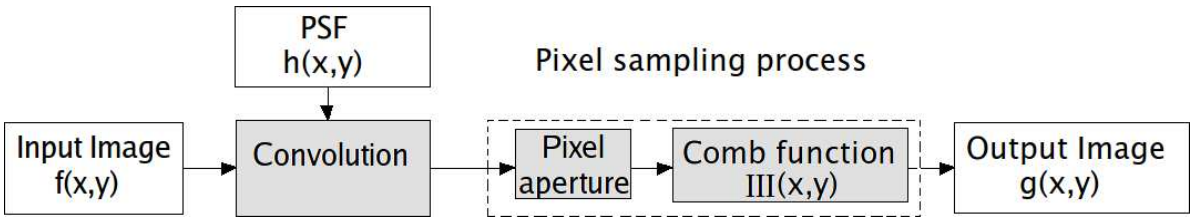

Figure 1. The physical imaging process. In the pixel sampling stage, the integration of the signal across the pixel aperture is followed by a comb function, $III(x,y)$, that samples this signal at a particular interval.

Figure 1 shows the imaging process of a physical imaging system which is discussed in detail below.

The MTF of a real imaging system can be experimentally assessed in various ways. One method (Samei et al. 1998) produces the 'presampled MTF' herein referred to as $H'(u,v)$, which includes the integrating effects from digital pixel sampling, $S(u,v)$, as well as those of the intrinsic physical blurring process, $H(u,v)$, associated with the imaging system itself (Dobbins 2000).

The presampled MTF is therefore given by:

$$H'(u,v) = H(u,v).S(u,v) \tag{3}$$

Pixel apertures are typically square, thus, the degradation process due to the integration of signal across the discrete pixel aperture (i.e. pixel sampling)can be modelled in the Fourier domain as a a product of two sinc functions:

$$S(u,v) = sinc(au).sinc(bv), \tag{4}$$

where a and b are the pixel dimensions, but usually $a = b$.

Providing the pixel sampling interval in the image is sufficiently small as not to introduce significant aliasing effects, then the effects of $S(u,v)$ can be considered insignificant on $H'(u,v)$. However, in practice, the digitisation process (pixel sampling) may well impact upon $H'(u,v)$. This aspect is explored below for the two principal approaches of image simulation described earlier: (i) synthesising realistic images from idealised representations of test objects; and (ii) synthesising images as if acquired on one imaging system from experimental images of another system.

2.2. Resolution modification of idealised images

Consider a digital image simulation chain where we start with an idealised image, $f(x, y)$, representing the pseudo-continuous case with very small, but finite pixel dimensions. We now wish to produce a representation of $f(x, y)$ as if it were acquired on an actual imaging system, using an experimentally acquired presampled MTF of a particular target imaging system A, with pixel dimensions $(\Delta x_A, \Delta y_A)$. Its presampled MTF can be written as:

$$H'_A(u, v) = H(u, v).S_A(u, v) \tag{5}$$

In order to correctly filter an idealised image, represented in the Fourier domain as $F(u, v)$, with the correct (blurring and sampling) processes represented by the presampled MTF, we use Equation 5

$$G_A(u, v) = F(u, v).H(u, v).S_A(u, v) \star III(u, v; \Delta x_A^{-1}, \Delta y_A^{-1}) \tag{6}$$

where the final image, $g_A(x, y) = FFT^{-1}[G_A(u, v)]$, and

$$S_A(u, v) = FFT(rect(\Delta x_A, \Delta y_A)). \tag{7}$$

The following constraint is assumed:

$$\Delta x_f = \Delta y_f \ll \Delta x_A = \Delta y_A \tag{8}$$

where $(\Delta x_f, \Delta y_f)$ is the pixel sampling of the original image array, $F(u, v)$, and $(\Delta x_A, \Delta y_A)$ is the pixel sampling of the target image array $G_A(u, v; \Delta x_A^{-1}, \Delta y_A^{-1})$, to be simulated. It is assumed in this work that the sampling interval is equal to the pixel size, which is consistent with current radiological imaging technology. However, if the image receptor's fill factor is small ($\leq 50\%$) then some further minor modification would be required. If $\Delta x \neq \Delta y$ then the resulting Fourier representations would no longer be isotropic. $III(u, v)$ is an array of delta functions separated by the reciprocal of the pixel pitch, i.e. the sampling comb (Giger & Doi 1984, Dobbins 2000, Gonzalez & Woods 2008). The effect of the sampling comb is to introduce an aliasing term, which is examined in section 3.3. However, as a practical rule of thumb, to minimise its effect to negligible levels, (Saunders & Samei 2003) recommend that to adequately represent an idealised image (Equations 1 and 2), then the pixel pitch $(\Delta x_f, \Delta y_f)$ in $f(x, y)$ must be $\leq 1/4$, but ideally $\leq 1/8$, times that of the target image sampling $(\Delta x_A, \Delta y_A)$. This resampling from the highly sampled $F(u, v)$ to that of $G_A(u, v)$ may be carried out in the Fourier domain with a sinc function filter, or in the spatial domain with neighbourhood averaging methods as these are equivalent operations (Parker et al. 1983, Press et al. 2002, Gonzalez & Woods 2008).

This theory is examined with respect to idealised images in Section 3. But before doing so, we show how to extend the above to correctly adjust pixel and MTF properties of experimental images acquired from one imaging system to appear as if acquired on another imaging system.

2.3. Experimental Image Synthesis

Consider an image system A, where $G_A(u,v) = F(u,v).H'_A(u,v) \star III(u,v;\Delta x_A^{-1}, \Delta y_A^{-1})$ and the associated presampled MTF is $H'_A(u,v)$ as shown in Equation 5. Starting with the Fourier representation of the experimental image, $G_A(u,v)$ and the associated presampled MTF, $H'_A(u,v)$, we wish to synthesize a new image, $G_B^A(u,v)$, as if it were acquired on some system B, with presampled MTF $H'_B(u,v) = H_B(u,v).S_B(u,v)$. In this case, $H_B(u,v)$ and $S_B(u,v)$ may or may not be equal to their respective counterparts in system A, but here we assume that pixel dimensions of system B are larger than in system A. To remove the effects of the presampled MTF of one system and replace with the other, we may simply write:

$$G_B^A(u,v) \approx G_A(u,v).\left(\frac{H'_B(u,v)}{H'_A(u,v)}\right) \star III(u,v;\Delta x_B^{-1}, \Delta y_B^{-1}) \tag{9}$$

$$\approx G_A(u,v).\left(\frac{H_B(u,v)}{H_A(u,v)}\right).\left[\left(\frac{S_B(u,v)}{S_A(u,v)}\right) \star III(u,v;\Delta x_B^{-1}, \Delta y_B^{-1})\right] \tag{10}$$

These last equations are given as approximations because it is impossible to undo the sampling in Equation 6 due to aliasing present in G_A from III_A. Specifically, Equations 10 omits the explicit effects of III_A as these are assumed to be negligible. The validity of this assumption is tested in Sections 3.2 and 3.3. In practice, $\left(\frac{S_B(u,v)}{S_A(u,v)}\right) \star III(u,v;\Delta x_B^{-1}, \Delta y_B^{-1})$ can be approximated with a resampling method such as weighted neighbourhood averaging and this is the approach adopted here (see section 2.4 below). Previous authors have presented related theory where the image was filtered with the ratio of presampled MTFs (Carton et al. 2005, Zanca et al. 2008), not the intrinsic MTFs as proposed here. However, this prior work cannot be directly applied when considering two systems with different pixel sizes. This is the case we address here. To demonstrate the validity to the above relationships, we consider several test cases in section 3.

2.4. Weighted Neighbourhood Averaging for Resampling

The aforementioned weighted neighbourhood averaging process was undertaken in the image domain. Image $g(x,y)$ is resampled from ideal image $f(x,y)$ as follows:

$$g(x,y) = \sum_{i,j=1}^{\lceil R \rceil} f(x_i, y_j).W_{i,j} \tag{11}$$

where R is the scaling ratio between sampling pitches of $f(x,y)$ and $g(x,y)$. The weighting $W_{i,j}$ is given by

$$W_{i,j} = \frac{p_i.p_j}{R^2} \tag{12}$$

p_i and p_j are the proportion of the pixel in image $f(x_i,y_j)$ that contributes to $g(x,y)$. This is clarified in Figure 2 for a scaling ratio of 2.6. Each pixel in $f(x_i,y_j)$ that contributes to a specific pixel in $g(x,y)$ is weighted based on the intersection of its area with the area of the new pixel. In the case where the $f(x,y)$ is another experimental

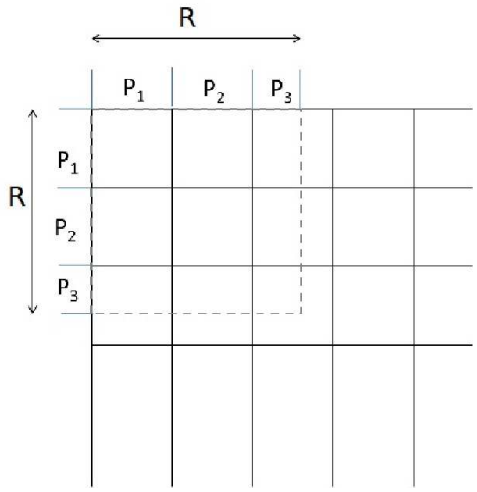

Figure 2. Weighted averages of each pixel in image $f(x, y)$ (solid grid) are calculated based on the area of the pixel that will be represented in $g(x, y)$ (dashed grid). Weighting for pixels $P_{1,1}$ to $P_{2,2}$ will equal $1/R^2$. Other pixels have a lower weight as only part of the pixel will contribute to $g(x, y)$.

image, the process of downsampling has a two-fold effect on the image: firstly, the image is filtered further by the ratio of $S_B(u, v)/S_A(u, v)$, the blurring is exaggerated when the two pixel sizes are not multiples of one another; and secondly, the image is sampled to correctly account for aliasing produced by the larger pixel sizes of $g_B(x, y)$. The validity of this is demonstrated in section 3.3.

3. Validation

To validate the method described in the previous section, idealised edge images, $f(x, y)$, were created with unit sampling $a = \Delta x_f = \Delta y_f$, which is assumed to be sufficiently fine so as not to affect subsequent measurements (Equation 8). Poisson noise was added to the idealised images and filtered using a modelled MTF such that the resultant relative noise was equal to 1% as would be expected in acquiring such an image experimentally from a typical mammography system. The MTF was defined by an error function following Burgess (1978). The filtered image was downsampled to multiples of a so as to represent examplar imaging systems A and B using the weighted neighbourhood averaging described in section 2.4. The presampled MTFs (Equation 6) were then measured(Samei et al. 1998) from these derived synthetic images and compared with the orignal model MTF. To model a clinical system, $H(u, v)$ can be derived from the clinical system's presampled MTF, $H'(u, v)$. Artefacts that arise from this process are usually minimised with the use of window functions. An alternative interpolation based method has been developed and is discussed in section 4.

3.1. Simulating images from an idealised image

Idealised edge images $f(x, y)$ (with pixel size of a) were filtered with model MTFs $H(u, v)$ for different radiographic imaging systems selected to represent a range of receptor performance. H was set to equal 0.5 at spatial frequencies 2.5, 7 and 15 c/mm. The resulting images were then sampled for system A with pixel size of $5a$ using methodology described in section 2.4 and the presampled MTF calculated for comparison with Equation 5. The results are shown in Figure 3. Case 1 where $H'(u, v)$ is dominated by the $S(u, v)$; case 3 where $H'(u, v)$ is dominated by $H(u, v)$ and case 2 which is intermediate to these. As may be expected, these demonstrate excellent agreement between the measured $H'_A(u, v)$ and that predicted by the convolution of $S_A(u, v)$ and $H_A(u, v)$ in Equation 6 for all cases. The average of the modulus of the relative difference between the measured $H'_A(u, v)$ and the predicted $H'_A(u, v)$ prior to the resampling stage was found to be less than 0.3%. After the resampling was applied the error was found to be 1.13%, 0.22% and 4.96% for cases 1, 2 and 3, respectively. Relative error increased at higher spatial frequencies where the MTF is smaller, with the largest relative deviation occurring for the poorest MTF (case 3) and the highest spatial frequencies.

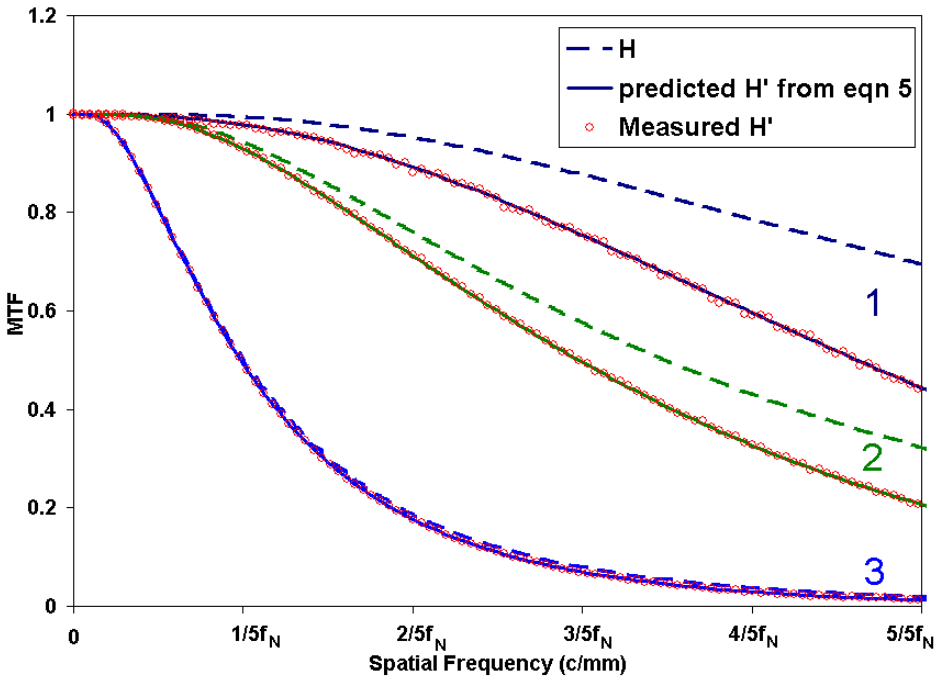

Figure 3. The intrinsic MTF (dashed curves), produced using a sampling aperture a was used to filter an edge image with sampling aperture $5a$. The resulting measured presampled MTF (red data points) demonstrates excellent agreement with the predicted presampled MTF (solid curves) using Equation 6. Three different cases are shown for illustration and are described in the text.

3.2. Simulating different systems

The method described in section 2.3 is examined here. X-ray images of an edge phantom were obtained from two mammography systems with the same beam quality and exposures. System A (Hologic Selenia) had a sampling interval of 0.07mm and system B (GE Essential) had a sampling interval of 0.10mm. Presampled MTFs were measured from the clinical systems to derive $H(u,v)$ for each system. To avoid any artefacts in the simulation process, $H(u,v)$ in each case was modelled as described in section 4. The image from system A was filtered as using the ratio of the *intrinsic* MTFs, $\left(\frac{H_B(u,v)}{H_A(u,v)}\right)$, in Equation 10 to produce a synthetic image representative of system B. The image, $G_B^A(u,v)$, was inverse Fourier transformed and resampled using weighted neighbourhood averaging. The resultant presampled MTF was measured and the result is presented in Figure 4.

The image from system A was filtered with ratio of the *presampled* MTFs, $\left(\frac{H'_B(u,v)}{H'_A(u,v)}\right)$. There is an excellent agreement between the presampled MTF of the experimental image from system B and the synthetic image for the same system when using the method proposed in this work. The alternative methodology (where the resampling stage is ignored) leads to a presampled MTF that had been underestimated at higher spatial frequencies. The average of the modulus of the relative difference across the spatial frequency range equal to 3.25% for the proposed method compared with 17.9% for the alternative method. As an implementation issue we also considered the effect of resampling the image with weighted neighbourhood averaging methods before or after the filtering process. Our empirical measurements from the simulated images suggested that there is slightly better agreement (approximately 2% improvement) between the final synthetic $H'(u,v)$ and the experimental $H'(u,v)$ if the resampling is carried out after the filtering process.

3.3. Investigation into the accuracy of resampling

The algorithm presented in section 2.4 is examined here. To assess whether the aliasing present in g_B^A differed greatly to that in g_B, an experiment was performed using images of discs. This experiment was repeated with and without noise. The noise was modelled using a Poisson distribution to approximate the system noise expected at typical clinical doses in mammography. The relative noise (ratio of standard deviation to mean intensity value) in the resultant images was approximately equal to 1.6% . Disc sizes ranged from 0.06 - 2.00 mm in diameter with equal contrast levels. The images were processed as outlined in Equation 5 to generate images for systems A and B. Images from system A were converted to appear as if acquired on system B using Equation 10 with weighted neighbourhood averaging. The ratio of the pixel sizes from system A to B was varied from 1:1.0 to 1:3.0 in 0.1 increments. Any differences between g_B and g_B^A are assumed to largely be due to errors in the weighted neighbourhood averaging methodology. Figure 5(a) shows an example of a residual difference image. The largest errors were at the edges of the discs. The standard deviation measured in the edge regions of the residuals

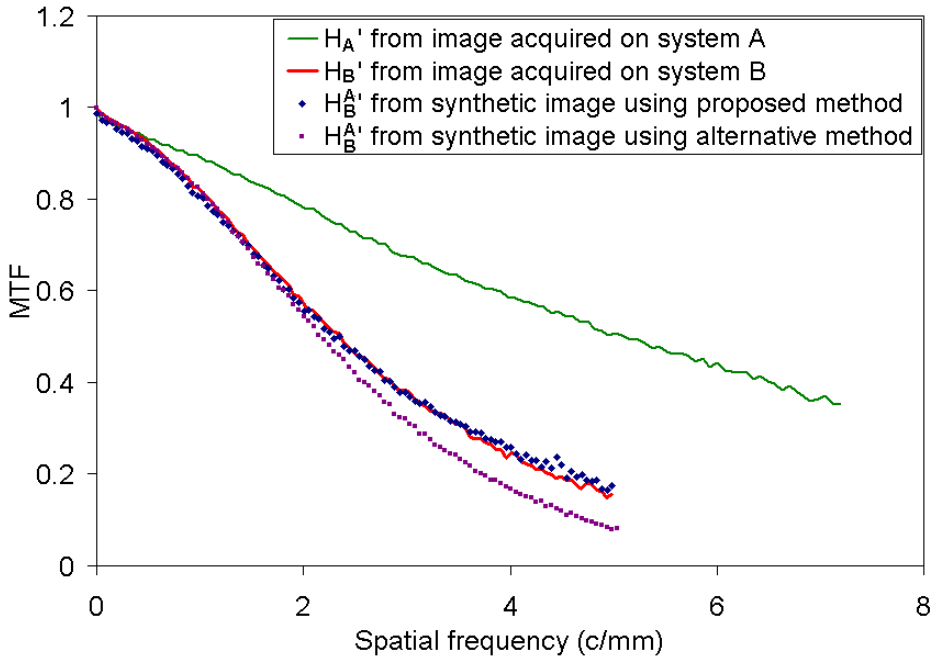

Figure 4. Presampled MTFs from system A, $H'_A(u,v)$, and B, $H'_B(u,v)$, shown in green and red, respectively. An edge image from system A was used to derive $G^A_B(u,v)$ using the method proposed in this work as well as with an alternative method. The MTF measured from the synthetic images are shown with blue and purple data points.

image was found to be less than 0.25% for images with noise added compared with 0.12% for the noiseless images. Figure 5(b) shows the variation of the standard deviation of the residuals with varying ratios of pixel sizes for the images with and without noise applied. The standard deviation of the residual difference is at its minimum for integer ratios of pixel sizes, increasing as the ratio deviates from the integer values in both cases. The standard deviation increases by more than two-fold when the noise is applied which is attributed to noise aliasing from higher spatial frequencies as might be present in real clinical images, although this is still a less than 1% effect.

Figures 6(a) to 6(f) show a close up illustration of the 2mm and 0.16mm discs for original, resampled and residual difference images for pixel size ratio 1:1.5. This shows that both discs have been visually well represented in this resampling process. Note that the main difference between original and resampled in the 2mm disc is confined to a small border region where the standard deviation of the residual difference range from -0.59 - 0.62% for the figures shown. In the case of 0.16mm disc, the standard deviation of the residuals are uniformally affected by statistical noise already present in the image, which range from -0.45 - 0.25%.

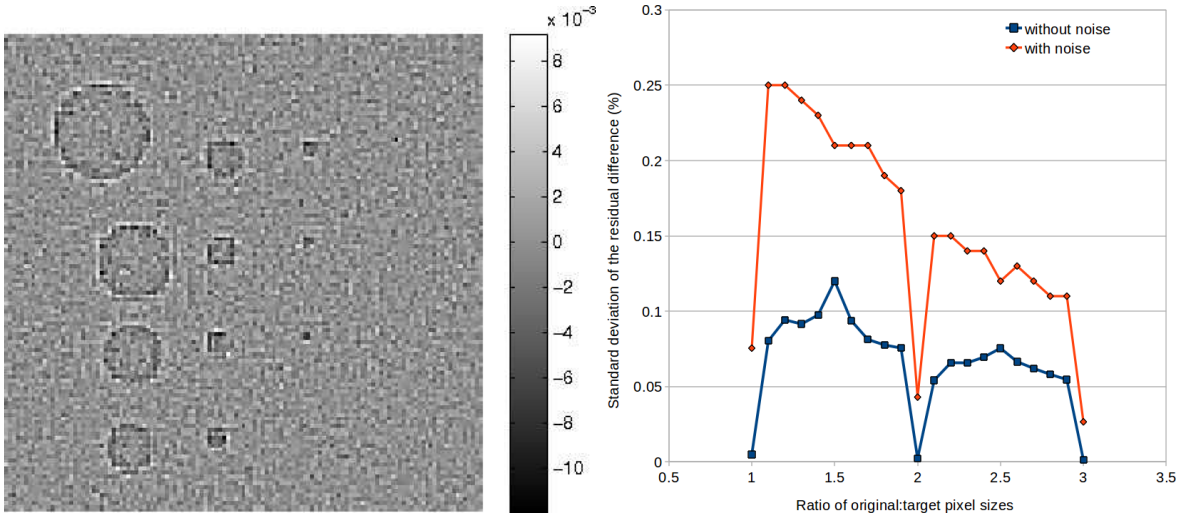

(a) Exemplar residual difference image

(b) Standard deviation of the residuals plot

Figure 5. (a) Relative residual difference image $(g_B - g_B^A)/g_B$ for pixel size ratio 1:1.5. (b) Standard deviation of the residual difference between $g_B(x, y)$ and $g_B^A(x, y)$ for a range of ratios of pixel sizes from system A.

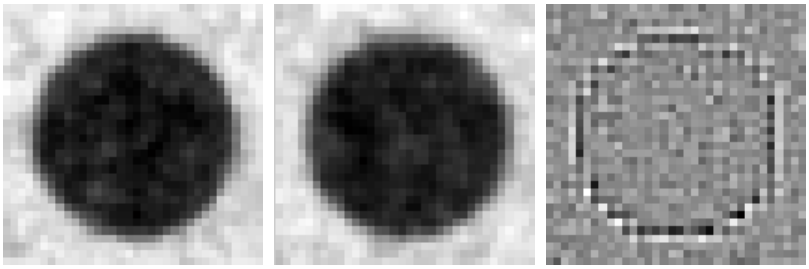

(a) g_B 2mm disc

(b) g_B^A 2mm disc

(c) Residual relative difference image of the 2mm disc

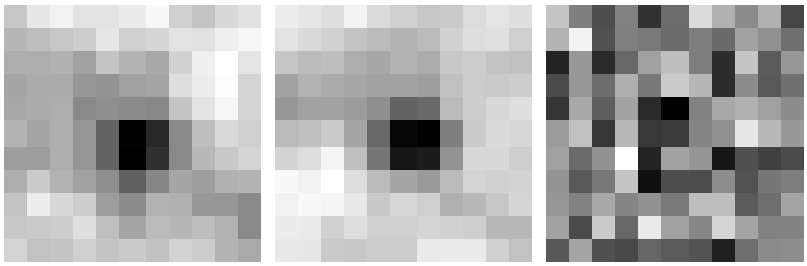

(d) g_B 0.16mm disc

(e) g_B^A 0.16mm disc

(f) Residual relative difference image of the 0.16mm disc

Figure 6. (a) and (d) g_B images of 2mm and 0.16mm discs, (b) and (e) g_B^A images of 2mm and 0.16mm discs, representing pixel size ratio 1:1.5. (c) and (f) residual relative difference images of 2mm and 0.16mm discs.

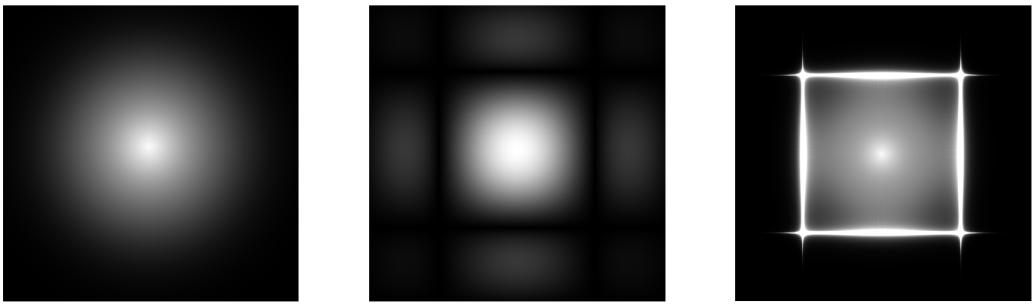

(a) $H'(u,v)$ (b) $S(u,v)$ (c) $H(u,v)$

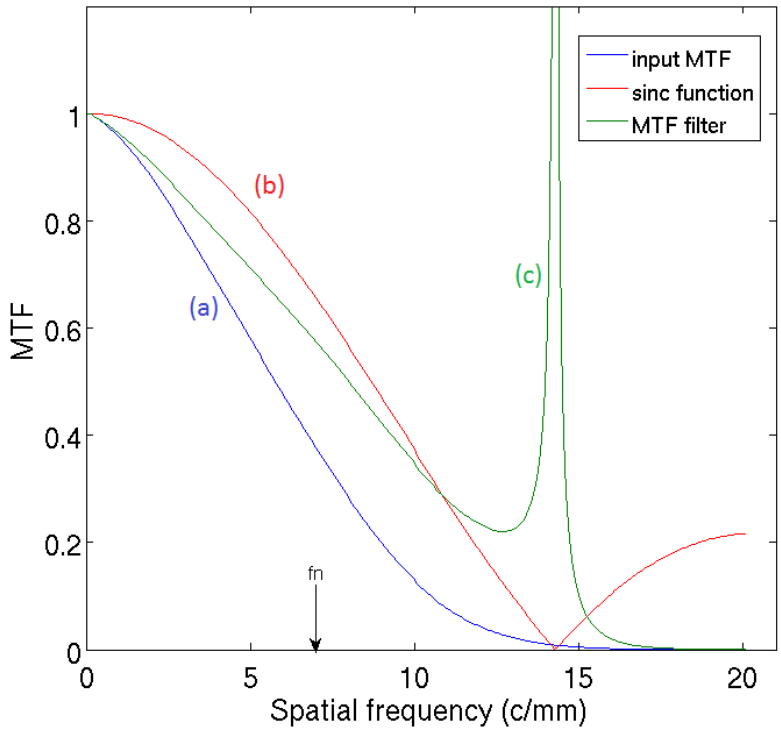

(d) Profiles

Figure 7. Effects of the sinc function on the presampled MTF. (a) is the presampled input MTF, (b) is the 2D sinc function corresponding to the original sampling of the presampled MTF, (c) is the resultant MTF filter, $H(u,v)$, after division of the input MTF by the sinc function. A clearer idea of the effects is shown in the 1D profile in (d) where the line plots correspond to the images (a) - (c).

4. MTF analysis

We now consider the effects of extracting the intrinsic MTF, $H(u,v)$ from the presampled MTF, $H'(u,v)$. We must match the range of the spatial frequency of the idealised image and $H(u,v)$ to filter the image correctly. This required a model of $H'(u,v)$ and $S(u,v)$ to be extended beyond that of the Nyquist frequency of the imaging receptor

as shown in Figure 7(a) and 7(b), respectively. $H(u, v)$ was derived from $H'(u, v)$ and $S(u, v)$. However, this process produces a sharp spike as shown in Figure **??** and 7(d). At high spatial frequencies, $H(u, v) \rightarrow 0$, but in the region where the sinc function approaches zero then a spike artefact is generated. This results in the derived $H(u, v)$ going to infinity. In the spatial domain this produces ringing, as the sinc function has considerable energy beyond the Nyquist frequency (Parker et al. 1983), causing extensive (and undesireable) artefacts (Saunders & Samei 2003, Workman 2005).

In order to prevent ringing artefacts, previous authors (Saunders & Samei 2003, Workman 2005, Parker et al. 1983) have suggested the use of a window function such as a Hann (or Hamming or Butterworth) window to force $H(u, v)$ to zero before the sinc function reaches zero. The limitation of this approach is that the window function needs to be configured individually for each system with a particular pixel size.

A more robust approach that removes the need for individual window functions is to adopt an interpolation based method. Assuming the intrinsic MTF, $H(u, v)$, is isotropic, the 1D presampled MTF was divided by the correct sinc function. This was then modelled in two ways: with a Hann window and fitted with a double Gaussian model, such that the model fitted smoothly through the spike. The modelled 1D profiles were interpolated into 2D $H(u, v)$ and used to filter separate idealised edge images and resampled to the pixel size of system A. For comparison purposes, an edge image was experimentally acquired on system A from section 3.2 and the presampled MTF was obtained (Samei et al. 1998). Figure 8 demonstrates the excellent agreement between the experiment and the two simulated (Hann/fitted) results. The Hann windowing method led to a synthetic $H'(u, v)$ that deviated by an average of the modulus of the relative difference $0.77 \pm 0.21\%$ from the experimentally acquired MTF. The Gaussian model method lead to a synthetic $H'(u, v)$ that deviated $0.46 \pm 0.19\%$. Although the performance of these two methods are equivalent, the approach offers a more convenient single step solution compared to use of windowing function, as the latter require individual manual adjustment to ensure $H(u, v)$ is forced to zero without introducing artefacts into the filter.

5. Discussion and Conclusion

The work presented here has described the correct use of the sampling process to be applied in a resolution modification process. Where a pixel dimension change is needed, alternative interpolation schemes may also be used for the downsampling stage, such as bilinear interpolation which then produce a $sinc^2$ function in the Fourier domain(Parker et al. 1983, Press et al. 2002) and Equations 3 - 10 would need to be appropriately modified. It must be borne in mind that this work describes an approximation to the real physical imaging chain, as it is not possible to completely remove the sampling effects in the original image. For the conversion of an image from one system to appear as if acquired on another system, the scope of this note is confined to the MTF modification and pixel sampling issues which are key steps in any image synthesis process. However,

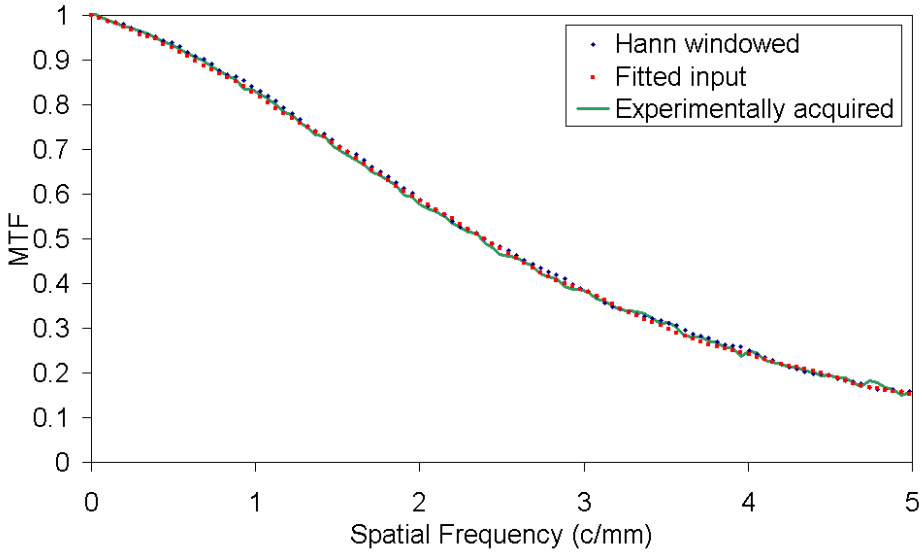

Figure 8. An example of the synthetic MTF derived from a Hann windowed MTF filter (blue points) compared with that derived from a Gaussian modelled MTF filter (red points). Both MTFs are compared with the experimentally acquired MTF modelled (solid green curve).

any such process will also need to account for further image degradation processes (e.g. beam hardening, noise sources, scatter and geometrical factors such as magnification, anti-scatter grid geometry, and in the case of tomosynthesis, X-ray tube projections etc.) dependent on the imaging system being considered, which is beyond the remit of this technical paper. The reader is directed to work that has been extensively covered by Mackenzie et al (Mackenzie et al. 2011) for further discussion on these aspects.

Acknowledgement

This work is part of the OPTIMAM project and is supported by the CR-UK & EPSRC Cancer Imaging Programme in Surrey, in association with the MRC and Department of Health (England). M.Y. also acknowledges support from an EPSRC Doctoral Training Grant.

References

Båth M, Håkansson M, Tingberg A & Månsson L 2005 Method of Simulating Dose Reduction for Digital Radiographic Systems *Radiation Protection Dosimetry* **114**(1-3), 253–259.

Carton A K, Vandenbroucke D, Struye L, Maidment A, Kao Y H, Albert M, Bosmans H & Marchal G 2005 Validation of MTF measurement for digital mammography quality control *Med. Phys.* **32**(6), 1684–1695.

Dobbins J 2000 *Handbook of Medical Imaging: Physics and Psychophysics* Chapter Image Quality Metrics for Digital Systems, pp. 161–222.

Giger M & Doi K 1984 Investigation of basic imaging properties in digital radiography. I. Modulation transfer function *Medical Physics* **11**, 287–295.

Gong X, Glick S, Liu B, Vedula A & Thacker S 2006 A computer simulation study comparing lesion detection accuracy with digital mammography, breast tomosynthesis, and cone-beam CT breast imaging *Medical Physics* **33**(4), 1041–1052.

Gonzalez R & Woods R 2008 *Digital Image Processing* 3rd edn Pearson Prentice Hall.

Grosjean B & Muller S 2006 Impact of Textured Background on Scoring of Simulated CDMAM Phantom *in* 'International Workshop of Digital Mammography 2006' Vol. 4046 pp. 460–467.

Mackenzie A, Workman A, Dance D, Yip M, Wells K & Young K 2011 Validation of a method to convert an image to appear as if acquired using a different digital detector *in* 'SPIE: Medical Imaging: Physics of Medical Imaging' Vol. 7961 pp. 159.

Parker J, Kenyon R & Troxel D 1983 Comparison of Interpolating Methods for Image Resampling *IEEE Transactions on Medical Imaging* **MI-2**(1), 31–38.

Press W, Teukolsky S, Vetterling W & Flannery B 2002 *Numerical Recipes in C* 2nd edn Cambridge University Press.

Ruschin M, Timberg P, Båth M, Hemdal B, Svahn T, Saunders R, Samei E, Andersson I, Mattson S, Chakraborty D & Tingberg A 2007 Dose dependence of mass and microcalcification detection in digital mammography: Free response human observer studies *Med. Phys.* **34**(2), 400–407.

Samei E, Flynn M & Reimann D 1998 A method for measuring the presampled MTF of digital radiographic systems using an edge test device *Med. Phys.* **25**(1), 102–113.

Samei E, Saunders R, Baker J & Delong D 2007 Digital Mammography: Effects of Reduced Radiation Dose on Diagnostic Performance *Radiology* **243**(2), 396–404.

Saunders R & Samei E 2003 A method for modifying the image quality parameters of digital radiographic images *Med. Phys.* **30**(11), 3006–3017.

Workman A 2005 Simulation of Digital Mammography *in* M Flynn, ed., 'SPIE: Medical Imaging: Physics of Medical Imaging' Vol. 5745 SPIE Bellingham, WA pp. 933–942.

Yip M, Lewis E, Young K & Wells K 2008 Validation of a digital mammography image simulation chain with automated scoring of CDMAM images *in* 'International Workshop on Digital Mammography' Vol. 5116 pp. 409–416.

Zanca F, Chakraborty D, Van Ongeval C, Jacobs J, Claus F, Marchal G & Bosmans H 2008 An improved method for simulating microcalcifications in digital mammograms *Med. Phys.* **35**(9), 4012–4018.

Zhou J, Zhao B & Zhao W 2007 A computer simulation platform for the optimization of a breast tomosynthesis system *Med. Phys.* **34**(3), 1098–1109.